IMPROVED SUSTAINABLE SANDWICH PANELS BASED ON BOTTLE CAPS CORE

Pablo Resende Oliveira[1,2], Michael May[1], Tulio Hallak Panzera[3*], Fabrizio Scarpa[4], Stefan Hiermaier[1,2]

[1] Fraunhofer EMI, Ernst-Mach Institut, Freiburg im Breisgau, Germany.

[2] Institute of Sustainable Systems Engineering, Albert-Ludwigs Universität Freiburg, Freiburg im Breisgau, Germany.

[3] Centre for Innovation and Technology in Composite Materials (CIT^{e}C), Department of Mechanical Engineering, Federal University of São João del Rei (UFSJ), Brazil.

Corresponding author[*]: panzera@ufsj.edu.br

[4] Bristol Composites Institute (ACCIS), University of Bristol, UK

Abstract: *A sandwich panel based on upcycled bottle caps core and sustainable components is investigated to contribute to advances in lightweight and environmentally friendly structural solutions. Ecological alternatives to the panel skin and adhesive, such as a recycled PET-bottle foil and a castor oil bio-polyurethane, respectively, are tested and compared to commercial components (aluminium skin and epoxy polymer). Bottle caps are characterised using a small punch test specially developed to obtain the properties of the bottle caps. Additionally, low-cost reinforcement (Portland cement) is added to adhesives to enhance the mechanical behaviour of the panel. The sustainable panels achieve enhanced efficiency compared to aluminium-based panels for core shear strength and stiffness, besides having similar specific flexural properties compared to those of epoxy-based PET panels. Despite their higher strength and stiffness, epoxy polymer-based panels show visible adhesive peeling off to bottle caps core and aluminium skin. In contrast, the biopolymer exhibits larger deformation and debonding of both substrates, indicating a progressive and ductile failure. The satisfactory efficiency of sustainable panels confirms the promising reuse of recycled bottle caps in structural applications.*

Keywords: sandwich panels, bottle caps, recyclability, design of experiment, bio-adhesive.

1. Introduction

Sandwich panels play a significant role in the field of lightweight structures due to their high crashworthiness, shear stiffness, and energy absorption capacity [1]. The panels are based on the bonding between a soft and thick core to outer skins made of strong and resistant materials, such as metals or composite laminates. The most classic sandwich panel design is based on the honeycomb core (HC), which is characterised by a cellular structure formed by bundled cells of same geometry [2]. The performance of HCs is highly dependent on material density, mechanical properties and the cell shape and arrangement [3]. Conventionally, hexagonal cell-based HCs are the most widely applied sandwich

core. However, alternative geometries have been tested, such as circular cell HCs and hybrid structures with circular cell inclusions and fillings [2-5].

Circular cell structures were first reported in the 1960s and thoroughly studied in recent years. Circular cells tend to have similar high energy absorption capacity, strength and toughness under out-of-plane loads [6, 7] compared to hexagonal cells [8, 9]. Circular tubes lead to greater buckling resistance, being able to withstand higher crushing loads and dissipate more energy. Some cell arrangements can be classified based on the angle between cells (Figure 1) [10]. Hexagonal packing (Figure 1b) has been considered the most promising design for energy absorption due to its improved structural constrains [11]. However, the efficiency of the structure is highly dependent on the shape of the cell wall, in which irregular structures (e.g. cells based on cone trunks instead of perfect cylinders) exhibit enhanced strength in cubic packing (Figure 1a) [12]. Circular cells also contribute to increased energy absorption capacity at higher crushing velocities in hybrid designs based on circular tube filled HCs [13], as well as reducing deflection of the back skin under impact with controllable deformation [14, 15], maintaining the survival space in vehicles during collision. The hierarchical addition of circular cells in square [16] and hexagonal HC cells joints [17] presented enhanced core energy absorption (up to 115% and 47.7%, respectively).

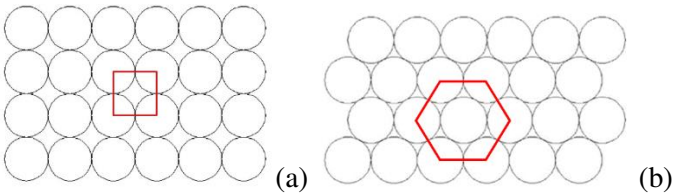

Figure 1. Cell packing arrangements for circular cell honeycomb: cubic (a) and hexagonal (b).

A critical aspect in structural design is its sustainable feature, e.g. the automotive sector is currently under strict environmental policy and low fuel consumption targets [18, 19]. A small amount of work on sustainable HC designs has been reported in the literature. Cabrera, Alcock and Pejis [20] developed a circular cell sandwich panel based only on polypropylene (PP) components. Thermoplastic panels achieved improved recycling but limited mechanical performance compared to recycled sustainable HC panels [12, 21]. These works [12, 21] used disposed bottle caps to build circular cell HC. The cap core was bonded to aluminium skins by synthetic thermosetting adhesive. The use of closed surface caps in alternated directions (Figure 2a) and with intra-cap adhesive connection promoted increased strength [21]. A larger amount of epoxy polymer (Figure 2b) stiffened the panel up to 92%, while providing higher specific properties. The improved flexural strength of the cubic packing has been attributed to the irregular shape of the lateral cap wall, which is similar to a cone trunk instead of a cylinder [12] (Figure 2c).

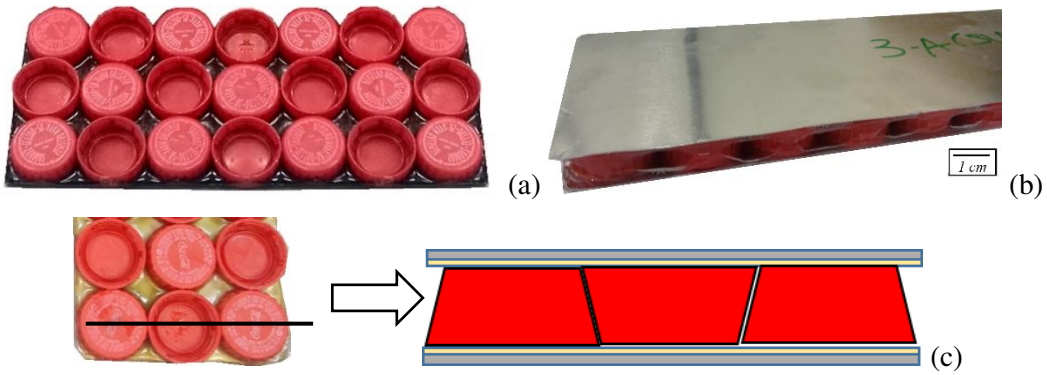

Figure 2. View of bottle caps honeycomb core with alternated configuration (a), manufactured samples with bottle caps (b), and cross-sectional diagram of alternated bottle caps panel (c).

HC made with bottle caps is highly promising due to its satisfactory strength and reduced environmental impact. Most recycling programmes do not include cap recycling, limiting the process to PET (Polyethylene terephthalate) bottles as they require different temperatures to be recycled [22]. Approximately 320,000 tons of bottle caps are disposed of in landfills annually [23], being one of the most commonly encountered items during cleaning works on seas and rivers [24]. The use of bottle caps in sandwich panels has been indicated as a promising route to upcycle the caps without requiring further modification on their structure [12, 21].

The use of petroleum-based polymers as adhesives undermines the ecological benefits of bottle caps panels. These adhesives can release hazardous fumes during curing, and are not biodegradable or from renewable sources. Many sustainable adhesives made from plant-oils have recently emerged. Different grains are tested as a source of oil [25-27], and castor oil is one of the main sources of ecological adhesives [28-30]. Despite their advantages, such as abundance, low-cost, low toxicity and biodegradability, the main disadvantage of plant-based adhesives is their poor mechanical performance and low metal bonding. The inclusion of fillers to adhesives aims to increase panel toughness and bonding without reducing mechanical strength [31-33]. Low cost fillers such as cement and recycled rubber particles have been added to bio-polyurethane adhesive for structural applications [34]. Cement particles enhanced polymer strength and stiffness by 55% and 183%, respectively. The rubber particles resulted in a biopolymer single lap strength increment of about 28%. T-peel tests revealed that the bonding capacity of the biopolymer was greater than the epoxy polymer, exhibiting progressive failure with almost three times greater displacement. A further limitation of bottle cap panels is the treatment required by metal skins for proper bonding, which may include mechanical grinding and the use of synthetic chemicals (e.g. primers) to enhance free surface energy. These treatments are difficult to apply and expensive, requiring extra steps and components. In addition, the use of synthetic primers can also cause damage to the manufacturer and the environment [31].

The literature review indicates that the use of reinforced biopolymer in sandwich structures is quite promising for secondary applications, such as transportation facilities, i.e. food truck floors and trains and buses side structures. In this context, the present work investigates improved sustainable

sandwich panels based on cement particle reinforced castor oil biopolymer. A novel recycled PET foil is also tested and compared to the aluminium skins. A 2^3 full factorial design is performed to identify the effects of adhesive type (epoxy polymer and castor oil biopolymer), skin material (aluminium and PET foil) and particle inclusions (no reinforcement and cement particles) on the physical and mechanical properties of sandwich panels.

2. Materials and methods

2.1 Materials

A two-component bio-polyurethane adhesive (AGT 1315) made from castor oil plant is supplied by Imperveg (Brazil). A mixed ratio of 1:1.2 by weight is considered. The Renlam-M epoxy system based on HY956 hardener is supplied by Huntsman (Brazil). A mixed ratio of 5:1 weight ratio (resin: hardener) is used. Aluminium (type AW-5754) is used as conventional skin. A PET foil made from recycled PET bottles (Armacell Benelux SCS – Belgium, thickness 1.3 mm) is used as sustainable skin. Portland cement (type ASTM III) from Holcim/Lafarge (Brazil) is used as received as adhesive filler. The core of the panel is based on disposed *Coca-Cola*^{TM} bottle caps of diameter ~ 30.3 mm made of HDPE and is carefully washed and dried for 24h prior to the manufacturing process.

2.2 Design of Experiment

Two experiments are conducted in this work. The first aims to determine the benefit over specific properties of increasing panel skin thickness. The aluminium skin panels of 1.0 mm and 1.5 mm thick combined with epoxy polymer (preliminary conditions C1' and C2') are compared to 0.5 mm skin thickness panels of previous studies [12, 21]. A second experiment, consisted of 2^3 full factorial design, evaluates the mechanical performance of sustainable sandwich panels. The effects of adhesive type (epoxy polymer and biopolymer), skin type (aluminium and PET foil) and particle reinforcement (without particle and with cement inclusions) on flexural properties are investigated. The thickness of the aluminium skins was chosen based on the highest specific properties obtained by independent preliminary testing. Cement particles are assessed as reinforcement based on the high strength and stiffness of the reinforced biopolymer [34]. Eight (8) conditions are manufactured for this experiment, as shown in Table 1. Four (4) samples are produced per experimental condition and per replicate with two (2) replicates, resulting in 8 samples per condition. The following factors are kept constant: the thickness of aluminium and PET foil (1 mm); amount of particle inclusion (3wt.% in accordance to previous studies [34]); time for mixing the polymer (2 minutes); curing conditions (28 days at room temperature ~24°C and ~55% relative humidity); cap type (caps from *Coca-Cola*^{TM} bottles) and the most adequate honeycomb packing system and configuration defined in previous studies (cubic packing in alternated directions [12, 21]).

Table 1. Project planning matrix, full factorial design 2^3.

Condition	Type of adhesive	Type of skin	Particle reinforcement
C1	Epoxy	Aluminium	No Particle
C2	Epoxy	Aluminium	Cement
C3	Epoxy	PET Foil	No Particle
C4	Epoxy	PET Foil	Cement
C5	Biopolymer	Aluminium	No Particle
C6	Biopolymer	Aluminium	Cement
C7	Biopolymer	PET Foil	No Particle
C8	Biopolymer	PET Foil	Cement

The properties obtained from the mechanical tests are submitted to the Design of Experiment (DoE) technique in Minitab v18 software [35], which verifies the influence of factors and interactions on the investigated responses within a 95% confidence interval, i.e. when its P-Value is less than or equal to 0.05 [36]. A factor interaction indicates that the effect of an individual factor depends on the level of another factor.

2.3 Components characterisation

The mechanical properties of skins under tensile tests are determined according to the ASTM E8 [37] protocol using an Instron 8801 machine. The adhesives were characterised in pristine (without reinforcement) and with reinforcement in a previous work [34]. The results of tensile strength and stiffness, impact resistance, single lap shear strength of pristine polymers and with reinforcement of 3 wt% are shown in Table 2.

Table 2. Mechanical and adhesion properties with standard deviation (in parenthesis) of pristine and reinforced epoxy and bio-polyurethane [34].

Type of Polymer	Type of Particle	Amount of Particle (%wt.)	Young's Modulus (GPa)	Tensile Strength (MPa)	Impact Resistance (kJ/m²)	Single Lap Strength (MPa)
Epoxy	-	-	1.9 (0.2)	30.8 (2.5)	15.8 (1.0)	3.9 (0.3)
Epoxy	Cement	3	2.6 (0.2)	38.0 (3.2)	12.3 (0.9)	3.7 (0.4)
Biopolymer	-	-	1.3 (0.1)	18.0 (0.8)	18.5 (1.3)	4.7 (0.4)
Biopolymer	Cement	3	1.9 (0.2)	30.8 (2.5)	15.8 (1.0)	3.9 (0.3)

Characterisation of the bottle cap core is a challenge due to the small sample size. The fabrication of larger samples by melting can induce possible chemical changes and affect results. The bottle caps were indirectly characterised by the hardness test [12]. Despite a good agreement with the results found in the literature, further cap characterisation is required. A small punch test based on the design reported by Mousa and Kim [38] is used to characterise discs taken from the bottom of the caps. A variety of properties are obtained in this test, such as average stiffness, fracture energy, maximum load and deformation. Figure 5 illustrates the design of the small punch test (Figure 5a) and the device (Figure 5b,c). In addition, following the guidelines of Bruchhausen *et al.* [39], estimated properties can be analytically predicted, such as yield stress and ultimate tensile strength. Optimised correlations are

shown in Equations 1 and 2 for yield stress and ultimate tensile stress, respectively. F_e and F_{max} refer to the load at the elastic-plastic transition point and the maximum load, respectively, while h_o is the disc thickness. The parameters α and β are correction factors dependent on the geometry of the test rig.

$$\sigma_y = \alpha_1 \cdot \frac{F_e}{h_o^2} + \alpha_2, \alpha_1 = 0.382 \; and \; \alpha_2 = 28.8 \quad (1)$$

$$\sigma_{UTS} = \beta_1 \cdot \frac{F_{max}}{h_o^2} + \beta_2, \beta_1 = 0.065 \; and \; \beta_2 = 268.81 \quad (2)$$

A disc size of Ø18 mm and 1.4 mm thick (Figure 5b) is placed in the centre of the lower die. A semi-spherical punch is connected to a test machine (Zwick Allroundline) equipped with a 250 kN load cell. The sample is compressed at 5 mm/min until the failure is detected, that is, reduction of the compressive load.

Figure 5. Small punch test cross-sectional drawing – units in mm (a), parts of the device (b) and mounted device (c)

2.4 Panel manufacturing and testing

The manufacturing process of the sandwich panels follows the guidelines of previous works [12,21]. The aluminium skins are degreased with liquid detergent and sanded in a ±45° direction (Figure 6a) to increase roughness and remove the oxide layer, which may reduce bond strength [40]. The skins are dried and acetone is spread over the surface for final cleaning. Unlike the previous study [12], synthetic primer is not considered in order to reduce the use of unsustainable components. PET foils are clean and sanded as surface treatment is not effective on polymers. The skins are laterally covered with a release tape and inserted into the mould to prevent polymer leakage (Figure 6b). The adhesive is prepared by mixing the polymer and the particles, spreading on the surface with a wooden stick. Subsequently, the caps are added until the skin is fully covered (Figure 6c). The mould is closed with a lid and the adhesive is left to cure for 24 h under constant pressure (~3 kPa). The partial sample is removed from the mould (Figure 6d) and the process is repeated to bond the second skin. The final sample is cured under pressure for an additional 24 h. The total curing time at room temperature (~24ºC)

and relative humidity (~55%) is 28 days. Figure 6e shows the samples produced. The sandwich panels have a dimension of approximately 240 × 90 mm². The thickness of samples varies between 13.5 mm and 15 mm, depending on the skins. Sample dimensions are based on ASTM C393 [41].

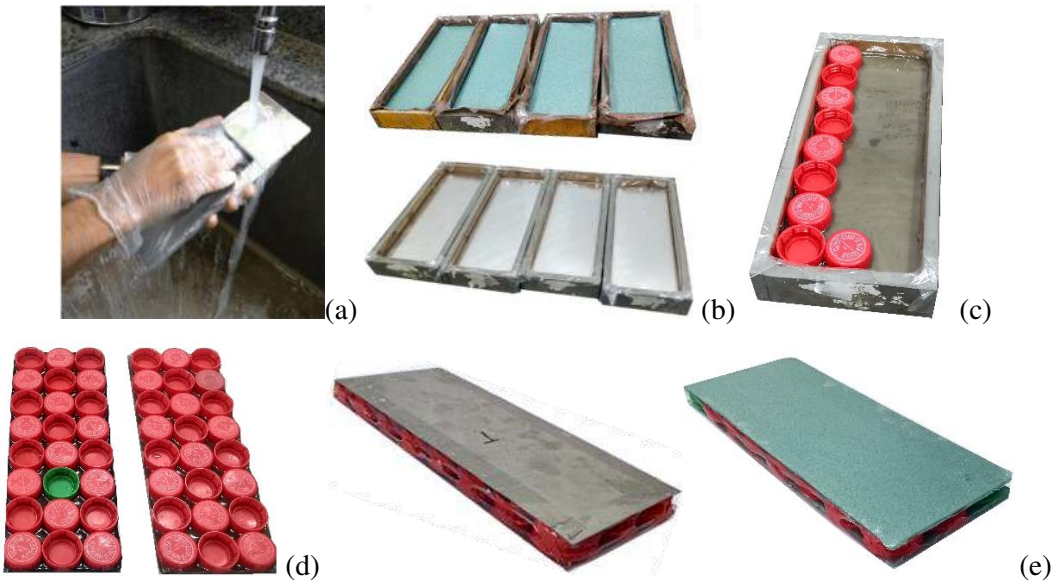

Figure 6. Manufacturing process of sandwich panels: cleaning process (a), insertion into moulds (b), caps bonding (c), partial produced samples (d), finished panels (e).

The panels are tested under 3-point bending load (3PB) on a 100 kN Shimadzu AGX test machine. The crosshead speed of 4 mm/min and span length of 150 mm are considered based on ASTM C393 [41]. The properties obtained are core shear stress (τ_c) (ASTM C393 [41]), core shear stiffness (G_c) (ASTM D7250 [42]), and flexural strength (σ_f) and stiffness (E_f) (ASTM D790 [43]). The calculation of the core shear properties considered the regular isotropic behaviour of the polymeric adhesive as the relevant core stiffness parameter, assumed as an approximation of the real core behaviour as indicated in previous works [12, 21]. The bulk density of the panels is also determined based on the apparent volume and weight obtained on a precision scale according to ASTM C20 [44].

Specific mechanical performance of the bottle cap panels is also calculated. Ashby [45] defined some optimisation indices to measure strength and stiffness efficiency to weight considering the sample shape. Equations (3) and (4) present the optimised indices for flexural modulus and strength of a sandwich panel. The terms E, σ, and ρ are the panel stiffness, panel strength, and bulk density, respectively.

$$E_{opt} = \frac{E^{1/3}}{\rho} \tag{3}$$

$$\sigma_{opt} = \frac{\sigma^{1/2}}{\rho} \tag{4}$$

3. Results

3.1 Components characterisation

Table 3 shows the properties of the skins. A significant reduction in panel strength, stiffness and density is observed for PET foil compared to aluminium skin. The results obtained by the punch test are presented in Table 4. A typical curve of the polymer samples is shown in Figure 7a. Four typical failure regions can be observed [38, 39]. The first region evidences the elastic deformation where the average stiffness of the plastic cap is calculated. The change in slope between regions I and II indicates a slight increase in deformation and the onset of plastic deformation. The third region corresponds to pure plastic deformation up to the maximum load. After the maximum load, a significant amount of energy is still achieved until the polymer rupture (region IV). Similar behaviour is shown by the other samples (Figure 7b).

Table 3. Properties of aluminium AW-5754 and PET foil

Property	**Aluminium AW-5754**		**PET foil**	
	Mean Value	SD	Mean Value	SD
Young's Modulus [GPa]	70.6	3.5	0.5	0.01
Tensile Strength [MPa]	246.6	3.2	6.9	0.2
Elongation at break [%]	16.2	0.5	33.9	2.7
Density [kg/m³]	2700	-	300	-

Table 4. Bottle cap properties estimated in small punch test.

Property	**Mean**	**SD**	**CV**
Maximum Force (F_m) [N]	384.5	5.8	1%
Elastic-plastic Transition force (F_e) [N]	35.0	2.9	8%
Average Stiffness [N/mm]	136.8	12.8	9%
Fracture Energy [J]	908.6	26.3	3%
Yield Stress (σ_y) [MPa]	34.7	0.6	2%
Ultimate Tensile Strength (σ_{UTS}) [MPa]	279.9	0.2	0%
SD = standard deviation and CV = coefficient of variation			

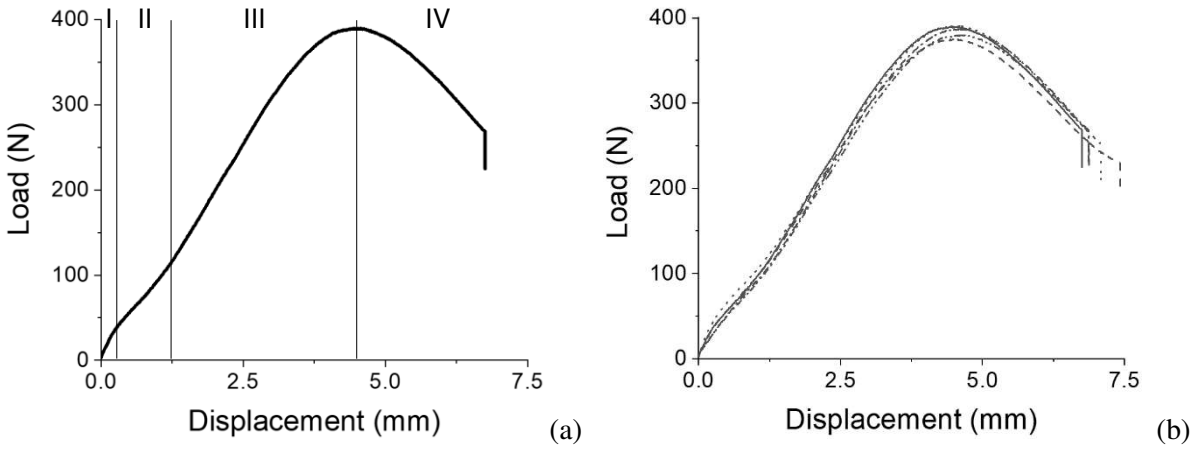

Figure 7. Typical behaviour obtained by the punch load test for caps discs (a) and curves of five samples (b).

3.2 Flexural test results

3.2.1 Evaluation of skin thickness effect

Table 5 shows the three-point bending properties for aluminium panels with different thicknesses (C1', 1.5 mm thick and C2', 1 mm thick). The flexural strength and stiffness of the panel and the shear strength and stiffness of the core are presented. Panel bulk density is also used to calculate specific properties. The results are analysed by Analysis of Variance and Tukey test techniques using Minitab v18. Tukey test reveal whether the analysed factor (skin thickness) significantly affects the investigated response. The P-Value less than 0.05 shown in bold in Table 6 [36] indicates that all responses are affected by the skin thickness factor. High values of R^2 (from 95.18 to 99.81%, Table 6) also indicate models well-adjusted to the experimental data [36]. Panels made of thicker skins exhibit higher strength (increases of about 17.1% in core shear strength and 6.1% in flexural strength). However, increasing skin thickness leads to reduced panel and core shear stiffness, with reductions of 11.8% and 7.0% in flexural modulus and core shear modulus, respectively. The 1.0 mm thick aluminium skins achieve greater strength and stiffness to weight ratio, with increments from 6.4% in core shear stress to 18.8% in flexural modulus. Based on these findings, 1.0 mm thick aluminium skins will be used in subsequent panels.

Table 5. Average and standard deviation (in parenthesis) results of the panel properties for independent testing of ANOVA of the influence of aluminium thickness.

	Absolute Properties					Weight-Specific Properties			
	τ_{core} **[MPa]**	G_{core} **[MPa]**	$\sigma_{flexural}$ **[MPa]**	$E_{flexural}$ **[GPa]**	ρ **[kg/m³]**	τ_{core} **[N.m/g]**	G_{core} **[N.m/g]**	$\sigma_{optimised}$ **[N.m/g]**	$E_{optimised}$ **[N.m/g]**
C1 (1.5mm)	1.2 (0.1)	36.4 (2.5)	32.3 (2.4)	3.8 (0.5)	829 (7.7)	1.3 (0.05)	4.0 (0.2)	6.8 (0.3)	18.8 (0.8)
C2 (1.0mm)	1.1 (0.1)	39.1 (2.9)	30.3 (3.2)	4.3 (0.1)	720 (7.6)	1.4 (0.06)	4.7 (0.2)	7.6 (0.3)	22.4 (0.7)

Table 6. DoE results for absolute and specific properties.

Factor	Absolute Properties				Weight-Specific Properties			
	τ_c	G_c	σ_f	E_f	τ_c	G_c	σ_{opt}	E_{opt}
Facing thickness (P-value ≤ 0.05)	**0.001**	**0.005**	**0.016**	**0.007**	**0.001**	**0.001**	**0.002**	**0.004**
R^2 (adj) (%)	99.63	98.55	95.18	97.97	99.81	99.70	99.29	98.91

Table 7 compares bulk density, flexural strength and stiffness of previous bottle cap panels [12] and the current conditions. The results show the skin with 1.0 mm thickness represent a suitable balance between structural efficiency and reduced risks of rupture under tensile stress.

Table 7. Comparison between conditions with different skin thicknesses.

Skin thickness	$\sigma_{optimised}$ **[MPa]**	$E_{optimised}$ **[GPa]**	ρ **[kg/m³]**
Aluminium 0.5 mm [12]	8.8	24.0	589

Aluminium 1.0 mm	7.6	22.4	720
Aluminium 1.5 mm	6.8	18.8	829

3.2.2 Absolute properties

Table 8 presents the results of the mechanical properties and bulk density of the panels. Data are statistically analysed by Design of Experiment (DoE) using Minitab v.18 software [35]. Table 9 shows the P-Values for the responses analysed. All factors and interactions less or equal to 0.05 are highlighted in bold. The effects of superior order are underlined and marked in italic, being analysed via interaction plots (Figures 8, 9). The interaction plots also show the results of the Tukey test to compare means between each interaction. The test attributes a letter (in this research, A to D, shown next to the value) for each interaction. The means that do not share a letter are significantly different from each other [36]. Table 9 also reports the R^2 (adj) values, which range from 99.98 to 99.99%, revealing an adequate fit of the experimental data to the statistical model. The Anderson-Darling normality test is also conducted and confirms the normality of the data, presenting P-Values greater than 0.05, as shown in Table 9 [36], which validates the ANOVA conclusions.

Table 8. Three-point bending properties and standard deviations (in parenthesis) - 2^3 factorial design.

	Absolute Properties					Weight-Specific Properties			
	τ_{core} [MPa]	**G_{core} [MPa]**	**$\sigma_{flexural}$ [MPa]**	**$E_{flexural}$ [GPa]**	**ρ [kg/m³]**	**τ_{core} [N.m/g]**	**G_{core} [N.m/g]**	**$\sigma_{optimised}$ [N.m/g]**	**$E_{optimised}$ [N.m/g]**
C1	1.1 (0.1)	39.1 (2.9)	30.3 (3.2)	4.3 (0.1)	720 (7.6)	1.4 (0.1)	4.7 (0.2)	7.6 (0.3)	22.4 (0.7)
C2	1.0 (0.1)	33.4 (2.7)	28.2 (3.0)	3.8 (0.3)	713 (6.5)	1.4 (0.1)	4.6 (0.2)	7.5 (0.4)	21.8 (0.7)
C3	0.3 (0.03)	11.6 (1.0)	6.7 (0.7)	0.4 (0.03)	403 (10.6)	1.3 (0.1)	5.6 (0.3)	6.4 (0.3)	18.0 (0.4)
C4	0.3 (0.05)	11.5 (0.6)	7.0 (0.8)	0.4 (0.03)	390 (12.3)	1.3 (0.1)	5.8 (0.3)	6.8 (0.8)	18.7 (0.6)
C5	0.4 (0.02)	5.2 (0.5)	10.1 (0.8)	0.7 (0.1)	643 (20.2)	0.9 (0.1)	2.7 (0.2)	4.9 (0.4)	13.3 (1.1)
C6	0.4 (0.05)	5.5 (0.5)	9.7 (1.0)	0.6 (0.1)	643 (7.5)	0.9 (0.1)	2.7 (0.1)	4.8 (0.3)	13.1 (0.5)
C7	0.2 (0.02)	2.0 (0.2)	4.3 (0.4)	0.2 (0.01)	339 (5.8)	1.2 (0.1)	3.7 (0.1)	6.1 (0.6)	15.3 (0.2)
C8	0.2 (0.01)	2.1 (0.1)	4.4 (0.4)	0.2 (0.01)	338 (4.3)	1.2 (0.1)	3.8 (0.1)	6.2 (0.5)	15.6 (0.4)

Table 9. DoE/ANOVA (2^3) for three-point bending properties.

	Factors	Absolute Properties				Weight-Specific Properties			
		τ_c	G_c	σ_f	E_f	τ_c	G_c	σ_{opt}	E_{opt}
P-Value ≤0.05	Type of Adhesive (TA)	**0.000**	**0.000**	**0.000**	**0.000**	**0.000**	**0.000**	**0.000**	**0.000**
	Type of Skin (TS)	**0.000**	**0.000**	**0.000**	**0.000**	**0.000**	**0.000**	**0.001**	**0.000**
	Particle reinforcement (PR)	**0.000**	**0.000**	**0.000**	**0.000**	0.184	0.098	0.125	0.700
	TA*TS	**0.000**	**0.000**	**0.000**	**0.000**	***0.000***	0.947	**0.000**	**0.000**
	TA*PR	**0.000**	**0.000**	**0.000**	**0.000**	0.720	0.076	0.561	0.934
	TS*PR	**0.000**	**0.000**	**0.000**	**0.000**	***0.002***	**0.002**	**0.000**	**0.001**
	TA*TS*PR	***0.000***	***0.000***	***0.000***	***0.000***	0.126	***0.005***	***0.030***	***0.036***
	R^2 (adj) (%)	99.99	99.98	99.98	99.99	99.43	99.87	99.62	99.79
	AD (P-Value ≥ 0.05)	0.914	0.145	0.314	0.324	0.992	0.447	0.310	0.920

Core shear strength and stiffness are analysed in a third-order interaction plot shown in Figures 8a and 8b. Aluminium skins provide greater core shear strength and stiffness than PET foil skins (Figure 8a and 8b, plot i), especially when combined with an epoxy polymer, with increases of 308% and 214%, respectively, which is associated higher strength of epoxy polymer and aluminium against shear loads. Biopolymer, on the other hand, exhibits increments limited to 159% in aluminium skins, due to its moderate strength to epoxy. Cement reinforcement combined with epoxy polymer slightly affects the core shear properties, achieving increases of 13% and 5% for core shear stiffness and strength, respectively (Figure 8a and 8b, plot ii). In contrast, the inclusion of fillers does not alter the properties of panels bonded to biopolymer, as well as panels based on PET foil skins (all means are in Group C – Figure 8a and 8b, plots ii and iii). Biopolymer panels exhibit 57% reduction in shear strength and 83% for shear stiffness.

The flexural behaviour of the panel (Figures 9a and 9b) also depends on the individual properties of the components, showing shear effects similar to the core (Figures 8a and 8b). The highest panel strength and stiffness is achieved when aluminium skins and epoxy adhesive are used, revealing increases of 326% and 945%, respectively, (Figure 9a and 9b, plot i) relative to recycled skins. Biopolymer-bonded panels also present up to 331% (Figure 9b, plot i) increase results with aluminium skins compared to PET. The moderate strength of biopolymer adhesive reduces bending properties in a similar way to core shear properties, i.e. 59% for strength and 69% for stiffness (Figure 9a and 9b, plot ii). The cement particles reduce the performance of the panel under 3PB loads when combined with epoxy polymers and aluminium skins due to the reduced interaction of epoxy-cement, while panels based on sustainable components are barely affected by particle reinforcement (Figure 9a.iii and 9b.iii).

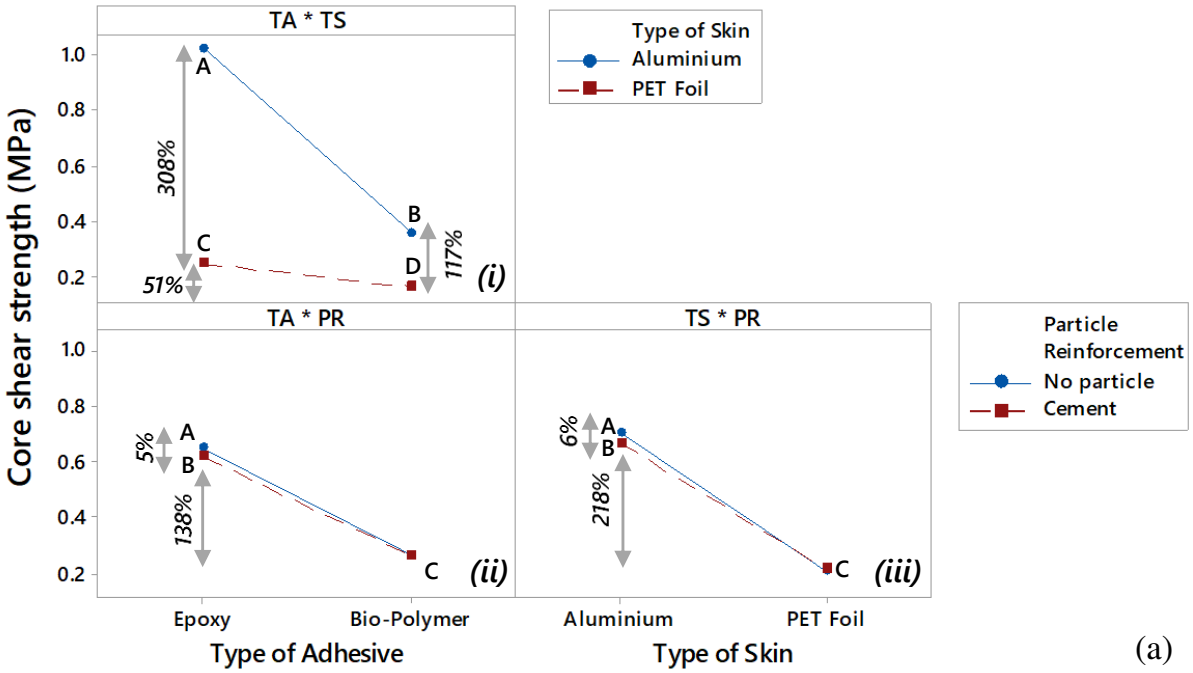

(a)

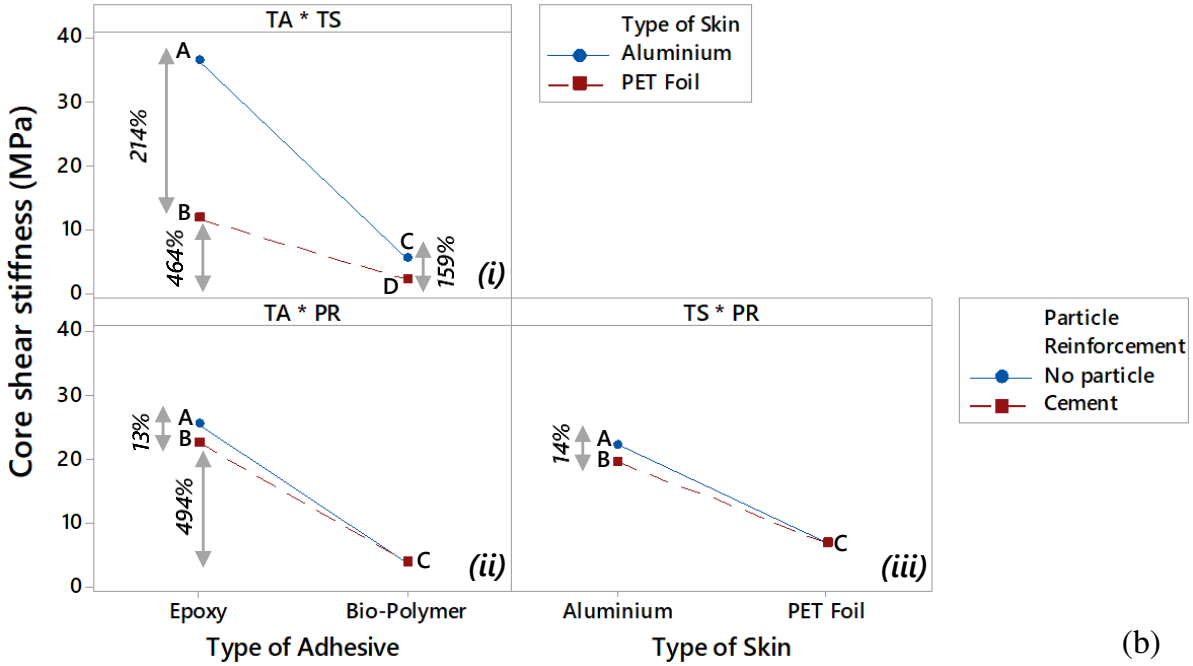

(b)

Figure 8. Third-order interaction plots for absolute core shear strength (a) and stiffness (b).

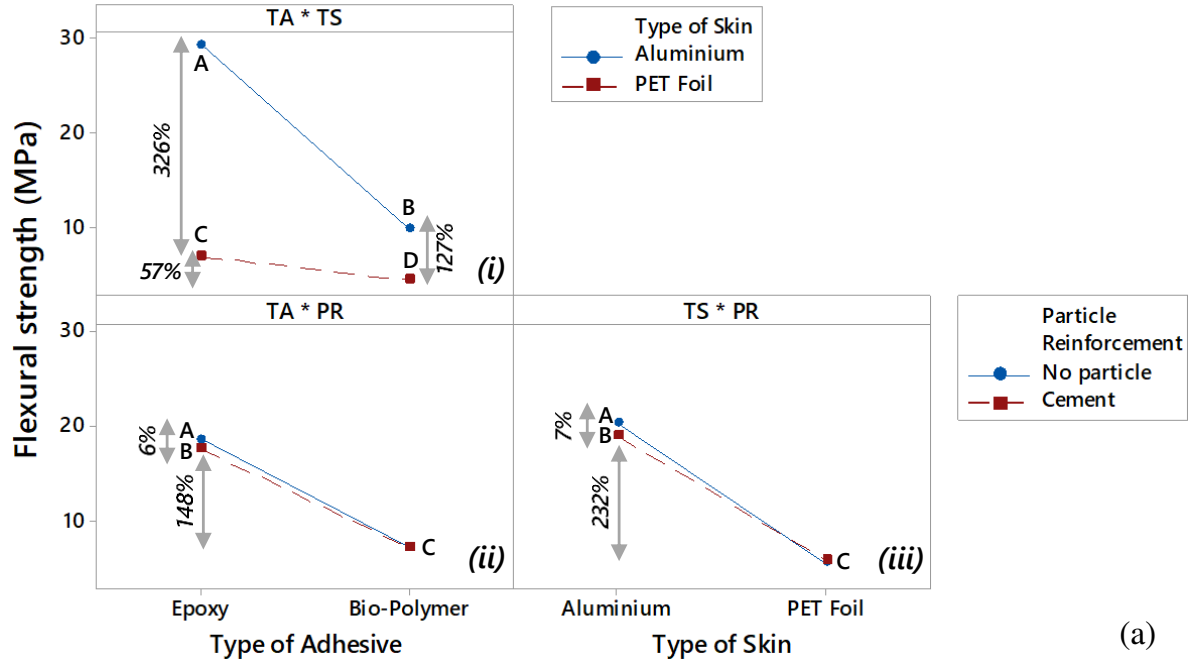

(a)

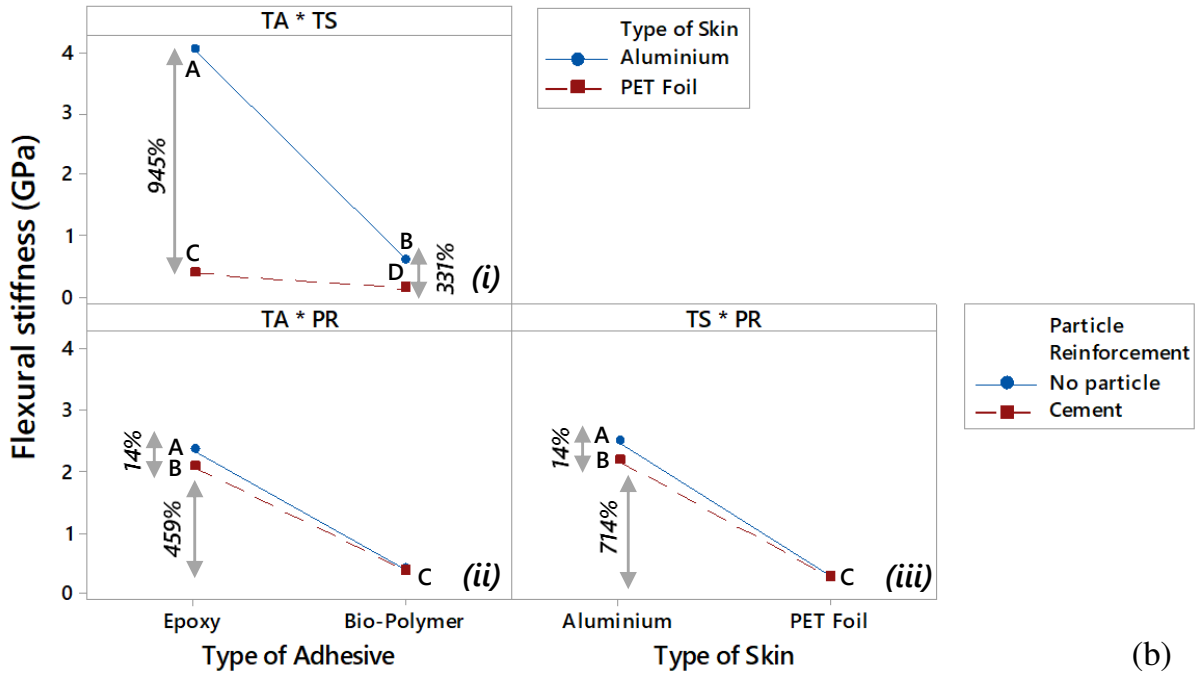

Figure 9. Third-order interaction plots for absolute flexural strength (a) and stiffness (b).

3.2.3 Flexural Specific properties

Specific properties of bottle cap panels, determined using Equations (3) and (4), highlight the effect of the proposed modifications on the efficiency of the structures. Table 8 also reports weight-balanced properties, while ANOVA analysis is shown in Table 9. R^2 (adj) values for specific properties range from 99.43 to 99.79%, which show well-fit data to the model. Specific data also follow the normal distribution according to the Anderson-Darling test with P-values greater than 0.05. Whereas core shear properties exhibit significant second-order interactions and main factor effects, flexural strength and stiffness show significant third-order interactions. Relevant factors and interactions are summarised in Figure 10.

Specific core shear strength exhibits two significant second-order interactions: "Type of adhesive vs. Type of skin" and "Type of skin vs. Particle reinforcement" (Figure 10a). The skin type has a strong effect with the adhesive type factor. Aluminium skin panels possess a specific strength 12% higher than that of PET foil when manufactured with epoxy polymer, while sustainable skin is 29% more efficient with biopolymer due to the reduced density of sustainable components (Figure 10a.i). A small difference is found for commercial and sustainable adhesive-bonded PET foil panels. The cement particles induce slight increases in the shear strength of the core with PET foil compared to aluminium, while the unreinforced panels show similar results for both skins, according to the Tukey´s test (Group B in Figure 10a.ii).

Core shear stiffness, specific flexural strength and stiffness are affected by a third order interaction shown in Figures 10b to 10d. The results evidence opposite effects for sustainable components. While PET foil panels provide a significant 23% increase in core shear stiffness, the use of bioadhesive

contributes to a substantial reduction in both skins (Figure 10b.i and ii). A slight interaction between skin and particle type is observed (Figure 10b.iii), having better results when PET foil is combined with cement reinforced adhesive, as shown by Group A (Tukey´s test). The results evidence a distinct behaviour between samples based on aluminium and PET-skin. The large difference in strength and stiffness of aluminium skin compared to bottle caps core and adhesive induces a panel response highly dominated by the performance of the skin, so aluminium panels do not benefit from a more rigid adhesive. PET-based panels, on the other hand, have a small difference between the properties of the skin and the core. Therefore, PET skin panels have a greater contribution of adhesive properties, exhibiting the greatest influence of particle reinforcement. Specific flexural strength and stiffness are higher for bioadhesive bonded PET panels than aluminium panels due to its lightweight design. Biopolymer-based panels are 26% and 17%, respectively, more efficient with PET foil regarding specific flexural strength and stiffness (Figure 10c and 10d, plot i). Aluminium skins increase mechanical panel efficiency by up to 20% with epoxy polymer. The use of biopolymer provides 22.5% and 29% reductions in specific strength and stiffness, respectively, over epoxy polymer, with no significant effect attributed to particle inclusion according to Tukey´s test (Figure 10c and d, plot ii). However, cement particles are relevant considering the combined effect with skin type factor (Figure 10c and d, plot iii). Specific strength shows 6% higher results for cement-reinforced PET-based panels, as discussed earlier, while 7% higher stiffness is achieved with unloaded aluminium skin panels.

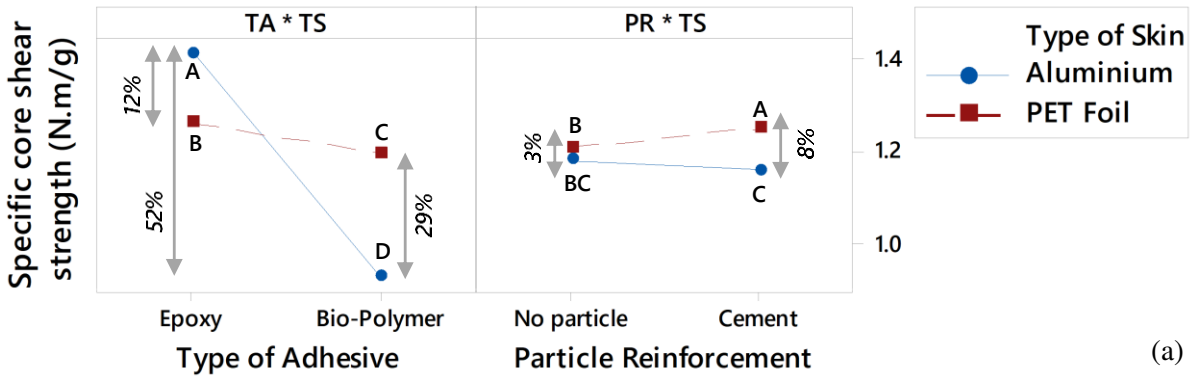

(a)

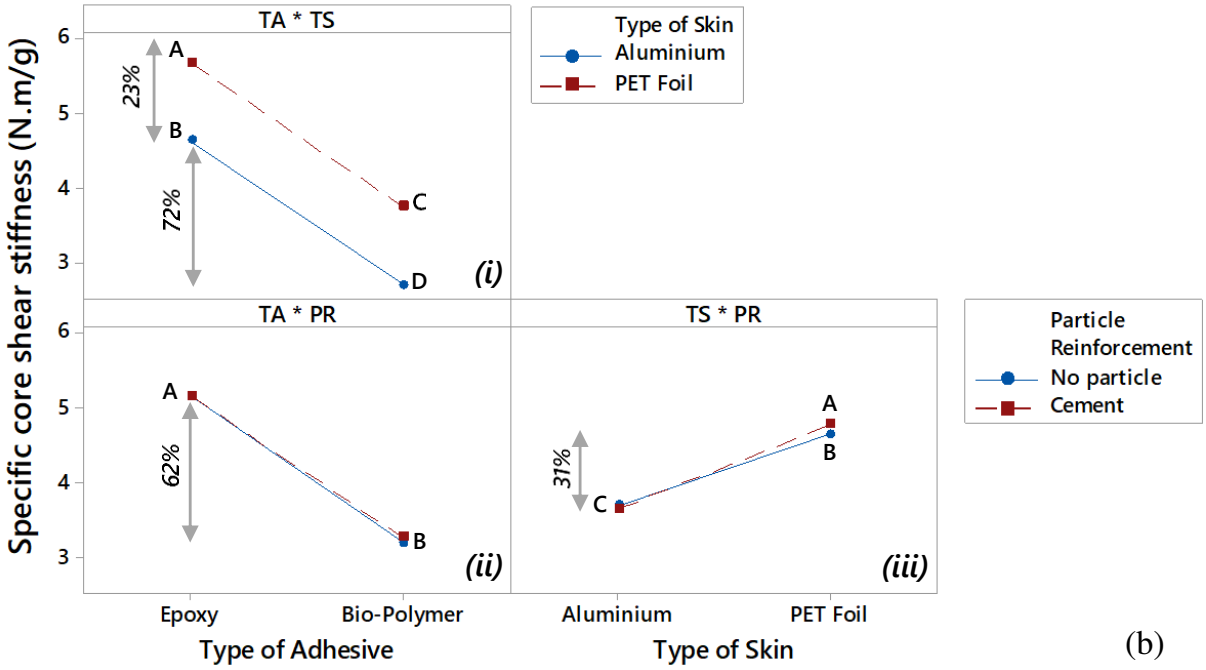
TA * TS
TA * PR
TS * PR
Type of Skin
Aluminium
PET Foil
Particle Reinforcement
No particle
Cement
Specific core shear stiffness (N.m/g)
23%
72%
62%
31%
(i)
(ii)
(iii)
Epoxy
Bio-Polymer
Type of Adhesive
Aluminium
PET Foil
Type of Skin

(b)

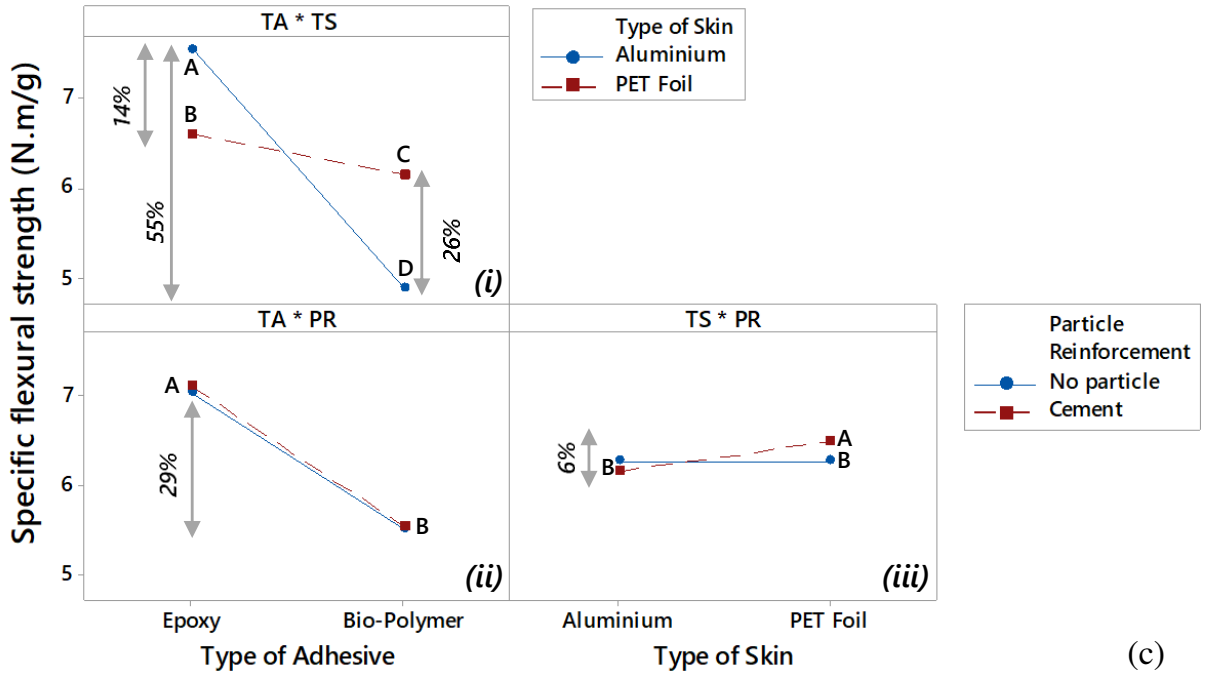
TA * TS
TA * PR
TS * PR
Type of Skin
Aluminium
PET Foil
Particle Reinforcement
No particle
Cement
Specific flexural strength (N.m/g)
14%
55%
26%
29%
6%
(i)
(ii)
(iii)
Epoxy
Bio-Polymer
Type of Adhesive
Aluminium
PET Foil
Type of Skin

(c)

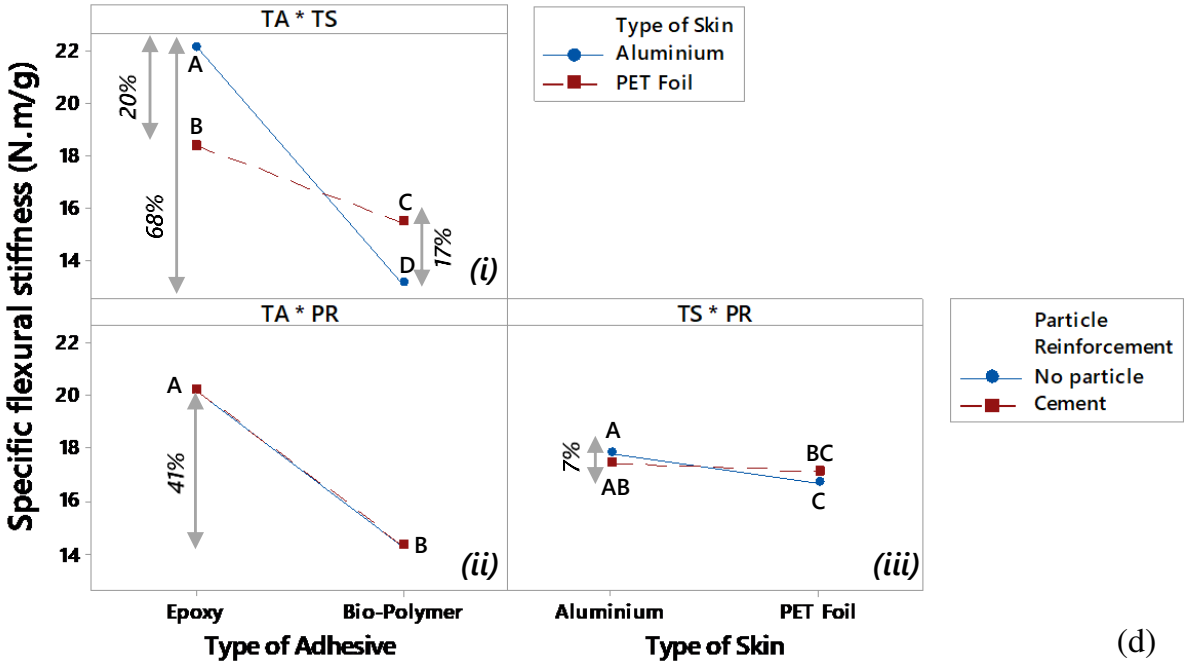

Figure 10. Main effect or interaction plots for specific responses: core shear strength (a) and stiffness (b), flexural strength (c) and stiffness (d).

3.3 Failure Analysis

Distinct failure modes are found depending on panel skins and adhesives. Figure 11 shows failure modes for each skin type and adhesive. Commercial components (aluminium skins and epoxy polymer) result in failure to bond bottle caps to the adhesive. Failure occurs by partial cracking of the adhesive and subsequent peeling. The failure is concentrated in a limited sample area, generally starting at the region with reduced bottle cap contact (open bottle cap side - Figure 11a). The absence of surface chemical treatment does not significantly affect failure compared to previous work [12]. PET foil skin and epoxy adhesive-based panels exhibit a sudden failure due to rupture of the lower region under tensile loads (PET skin and adhesive layer). The maximum strength of the sample under tensile loads (under neutral line) is not limited to the maximum PET skin strength, as shown in Table 3. Instead, the PET foil is extended until the adhesive is debonded from the plastic caps in a load inferior to the polymer ultimate tensile strength (shown in Table 1), leading to simultaneous core and skin rupture. The crack propagates along the width direction around the edges of the caps (Figure 11b), with adhesive rupture and debonding of the adjacent row of caps.

In contrast, the biopolymer adhesive leads to progressive failure for both skins. The biopolymer bonded aluminium skins achieve the largest deformation with marginal debonding between the open end of a bottle cap and the adhesive (Figure 11c). Adhesive peeling on the open cap side results in a slight reduction in flexural loading and ductile deformation, promising behaviour with respect to the safety of the structure. PET biopolymer based panels do not exhibit skin rupture. Instead, the upper skin wrinkles [2] attributed to the buckling effect due to compressive loads, while the skin under tensile loads exhibits a significant elongation without any rupture and slight increment from the maximum skin

strength due to the core behaviour. Skin buckling also resulted in local skin-adhesive debonding in some samples (Figure 11d).

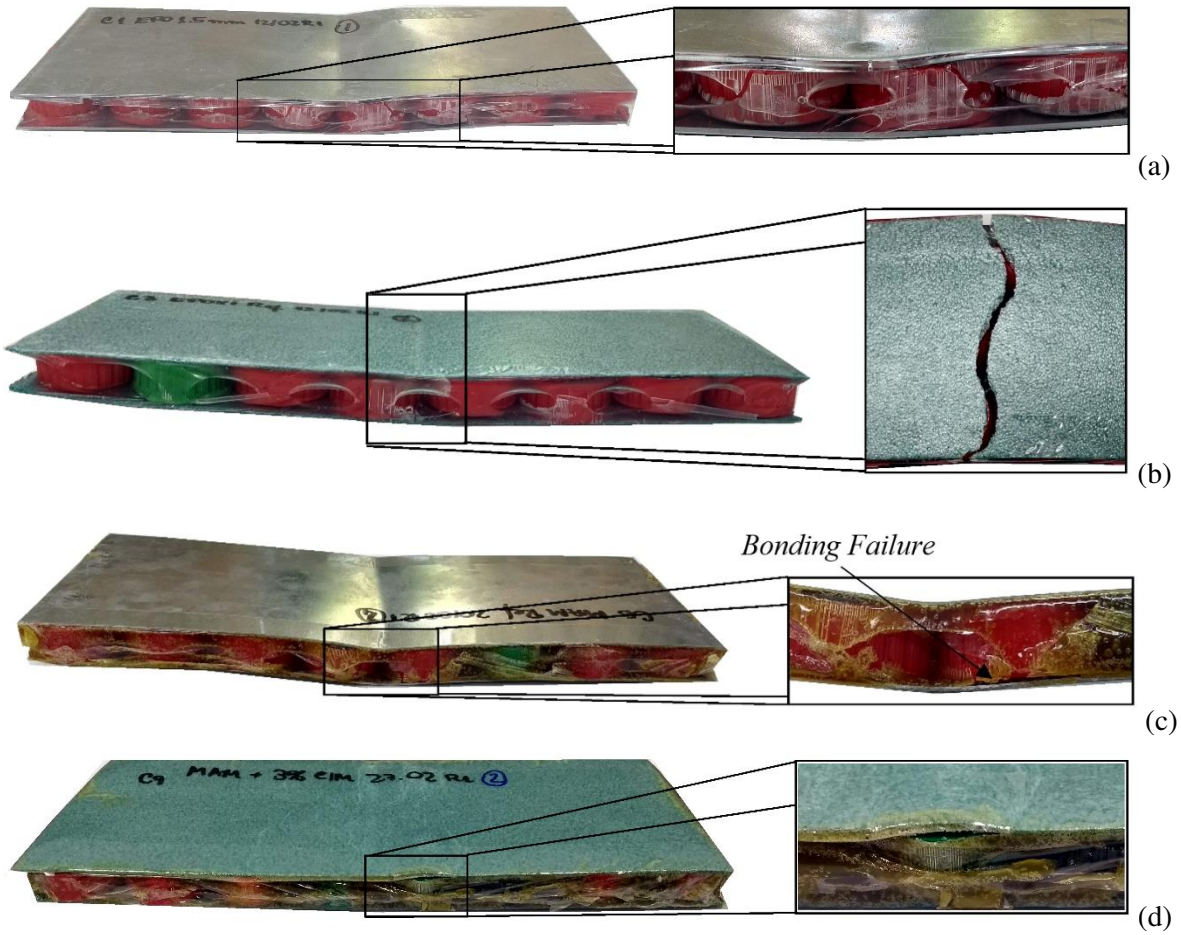

Figure 11. Failure mode of different configurations of bottle cap panels: epoxy polymer with aluminium (a) and PET skins (b), biopolymer with aluminium (a) and PET skins (b).

3.4 Comparative Analysis

Table 10 shows a comparison between the main properties of the proposed honeycomb panels and an all-aluminium based honeycomb designed for airplane structure (Gillfloor 5424), used the aisle and cargo floors of a Boeing 737-800 aircraft [46]. The proposed bottle caps core with aluminium skins and epoxy polymer exhibits 39% increased absolute flexural properties compared to the panel based on aluminium honeycomb. Akatay *et al.* [46] reported the absolute properties and the weight per unit area of the panel. Considering the thickness of the panel, an approximate equivalent density of the sandwich panel is determined, from which the specific flexural stiffness can be estimated. The approximate result in Table 10 shows a superior weight-specific performance of the aluminium honeycomb panels. The proposed bottle cap panel has 45% flexural stiffness of the aerospace honeycomb when manufactured in aluminium skins and 27% of the specific stiffness when manufactured in PET foil. It is a remarkable result, considering the basic inexpensive and eco-friendly core component proposed.

Table 10. Comparison between the proposed panels and the all-aluminium panel.

Type of panel	$E_{flexural}$ [GPa]	ρ [kg/m³]	$E_{optimised}$ [N.m/g]
Panel with Al skins + Epoxy Adhesive (C1)	4.3 (0.1)	720 (7.6)	21.8 (0.7)
Panel with Al skins + Biopolymer (C5)	0.7 (0.06)	643 (20.2)	13.3 (1.1)
Panel with CFRP skins + Al- honeycomb [46]	3.1 (0.03)	303	*48.1*

4. Conclusions

A sustainable sandwich panel based on bottle caps is investigated. New sustainable components, such as a recycled PET-based skin and a castor-based bio-polyurethane adhesive, are tested against classic components (aluminium skin and epoxy polymer) via a full factorial design. The effect of particle inclusions (cement particles) on the mechanical properties and panel toughness is also investigated. The main conclusions are summarised below:

i. PET foil skin is 29% and 32% more efficient than aluminium in biopolymer-based panels for core shear strength and stiffness, respectively. Specific flexural properties of biopolymer-based samples obtain higher results for PET than aluminium skins. Both adhesives achieve similar results along with PET skins;

ii. Particle inclusions have a substantial effect on the absolute core shear and flexural properties. In contrast, cement inclusions increase specific core shear and flexural strength of PET-based samples by 6 and 8% from pristine adhesive-based panels, respectively;

iii. Biopolymer adhesive provides reduced panel strength and stiffness compared to epoxy polymer. However, the sustainable adhesive exhibits better interaction with the recycled skin and core, resulting in progressive failure and marginal skin-core-adhesive debonding. The epoxy polymer leads to debonding of the aluminium skin and the rupture of the PET foil.

The findings highlight the feasibility of the proposed modifications towards the development of a more sustainable sandwich panel structure based solely on sustainable components. The resulting material keeps the easy manufacturing process and reduces the impact of non-sustainable components using recycled skin and a bio-sourced adhesive. This research presents new possibilities for the composition of bottle cap panels with more sustainable components, this topic being the scope of future research.

ACKNOWLEDGEMENTS

The authors acknowledge the support of CNPq-Brazil (PhD Scholarship 290224/2017-9 and PQ-309885/2019-1) and the donations from Armacell Benelux SCS (Belgium) and Imperveg Company (Brazil).

REFERENCES

1. Lu G, Yu T. Composite materials and structures. Energy Absorption of Structures and Materials 2003:317–50. doi:10.1533/9781855738584.317.
2. Bitzer TN. Honeycomb Technology: Materials, Design, Manufacturing, Applications and Testing. Dordrecht: Springer Netherlands; 2012.
3. Gibson LJ, Ashby MF. Cellular solids: Structure and properties, 2nd Ed., Cambridge: Cambridge University Press; 1997.
4. Wang Z. Recent advances in novel metallic honeycomb structure. Composites Part B: Engineering 2019;166:731–41. doi:10.1016/j.compositesb.2019.02.011.
5. Birman V, Kardomateas GA. Review of current trends in research and applications of sandwich structures. Composites Part B: Engineering 2018;142:221–40. doi:10.1016/j.compositesb.2018.01.027.
6. Pehlivan L, Baykasoğlu C. An experimental study on the compressive response of CFRP honeycombs with various cell configurations. Composites Part B: Engineering 2019;162:653–61. doi:10.1016/j.compositesb.2019.01.044.
7. Linul E, Serban DA, Marsavina L. Influence of Cell Topology on Mode I Fracture Toughness of Cellular Structures. Physical Mesomechanics 2018;21:178–86. doi:10.1134/s1029959918020121.
8. Oruganti R, Ghosh A. FEM analysis of transverse creep in honeycomb structures. Acta Materialia 2008;56:726–35. doi:10.1016/j.actamat.2007.10.019.
9. Lin T-C, Chen T-J, Huang J-S. In-plane elastic constants and strengths of circular cell honeycombs. Composites Science and Technology 2012;72:1380–6. doi:10.1016/j.compscitech.2012.05.009.
10. Gotkhindi TP, Simha K. In-plane effective shear modulus of generalized circular honeycomb structures and bundled tubes in a diamond array structure. International Journal of Mechanical Sciences 2015;101-102:292–308. doi:10.1016/j.ijmecsci.2015.08.009.
11. Hu L, He X, Wu G, Yu T. Dynamic crushing of the circular-celled honeycombs under out-of-plane impact. International Journal of Impact Engineering 2015;75:150–61. doi:10.1016/j.ijimpeng.2014.08.008.
12. Oliveira PR, Panzera TH, Freire RT, Scarpa F. Sustainable sandwich structures made from bottle caps core and aluminium skins: A statistical approach. Thin-Walled Structures 2018;130:362–71. doi:10.1016/j.tws.2018.06.003.
13. He Q, Feng J, Zhou H, Tian G. Numerical study on the dynamic behavior of circular honeycomb structure with concentrated filling inclusions defects. Journal of Mechanical Science and Technology 2018;32:3727–35. doi:10.1007/s12206-018-0725-4.
14. Liu J, Wang Z, Hui D. Blast resistance and parametric study of sandwich structure consisting of honeycomb core filled with circular metallic tubes. Composites Part B: Engineering 2018;145:261–9. doi:10.1016/j.compositesb.2018.03.005.
15. Wang Z, Liu J. Numerical and theoretical analysis of honeycomb structure filled with circular aluminum tubes subjected to axial compression. Composites Part B: Engineering 2019;165;626–635. doi:10.1016/j.compositesb.2019.01.070.

16. Wu Y, Fang J, He Y, Li W. Crashworthiness of hierarchical circular-joint quadrangular honeycombs. Thin-Walled Structures 2018;133:180–91. doi:10.1016/j.tws.2018.09.044.
17. Hu D, Wang Y, Song B, Dang L, Zhang Z. Energy-absorption characteristics of a bionic honeycomb tubular nested structure inspired by bamboo under axial crushing. Composites Part B: Engineering 2019;162:21–32. doi:10.1016/j.compositesb.2018.10.095.
18. Kim J-K, Yu T-X. Forming and failure behaviour of coated, laminated and sandwiched sheet metals: a review. Journal of Materials Processing Technology 1997;63:33–42. doi:10.1016/s0924-0136(96)02596-4.
19. May M, Hesebeck O. Assessment of experimental methods for calibrating rate-dependent cohesive zone models for predicting failure in adhesively bonded metallic structures. Engineering Failure Analysis 2015;56:441–53. doi:10.1016/j.engfailanal.2014.12.008.
20. Cabrera N, Alcock B, Peijs T. Design and manufacture of all-PP sandwich panels based on co-extruded polypropylene tapes. Composites Part B: Engineering 2008;39:1183–95. doi:10.1016/j.compositesb.2008.03.010.
21. Oliveira PR, Bonaccorsi AMS, Panzera TH, Christoforo AL, Scarpa F. Sustainable sandwich composite structures made from aluminium sheets and disposed bottle caps. Thin-Walled Structures 2017;120:38–45. doi:10.1016/j.tws.2017.08.013.
22. Aver K. 360: Bottle Caps, Earth911. 2009. <http://www.earth911.com/food/360-bottle-caps/>. Accessed: 07 June 2019.
23. Recycling NJ. Bottle cap recycling (plastic and metal) in New Jersey. 2016. <http://www.recyclingnj.com/recycle/caps.html> Accessed: 07 June 2019.
24. Boonstra M, van Hest F. The findings of the first survey into plastic bottle cap pollution on beaches in the Netherlands. The North Sea Foundation, Netherlands. 2017. <http://www.noordzee.nl/project /userfiles// SDN_Doppenrapport_EN_2017_DEF_small.pdf> Accessed: 07 June 2019.
25. Xing J, Li T, Yu Y, Chen C, Chang J. Development and characterization of a new bio-adhesive for wood using cassava starch and bio-oil. International Journal of Adhesion and Adhesives 2018;87:91–7. doi:10.1016/j.ijadhadh.2018.09.005.
26. Bacigalupe A, Solarte AMF, Fernández MA, Sánchez RMT, Eisenberg P, Escobar MM. Bio-adhesives from soy protein concentrate and montmorillonite: Rheological and thermal behaviour. International Journal of Adhesion and Adhesives 2017;77:35–40. doi:10.1016/j.ijadhadh.2017.03.018.
27. Zain NM, Roslin EN, Ahmad S. Preliminary study on bio-based polyurethane adhesive/aluminum laminated composites for automotive applications. International Journal of Adhesion and Adhesives 2016;71:1–9. doi:10.1016/j.ijadhadh.2016.08.001.
28. Moghadam PN, Yarmohamadi M, Hasanzadeh R, Nuri S. Preparation of polyurethane wood adhesives by polyols formulated with polyester polyols based on castor oil. International Journal of Adhesion and Adhesives 2016;68:273–82. doi:10.1016/j.ijadhadh.2016.04.004.

29. Tenorio-Alfonso A, Pizarro M, Sánchez M, Franco J. Assessing the rheological properties and adhesion performance on different substrates of a novel green polyurethane based on castor oil and cellulose acetate: A comparison with commercial adhesives. International Journal of Adhesion and Adhesives 2018;82:21–6. doi:10.1016/j.ijadhadh.2017.12.012.
30. Raghunanan LC, Fernandez-Prieto S, Martínez I, Valencia C, Sánchez MC, Franco JM. Molecular insights into the mechanisms of humidity-induced changes on the bulk performance of model castor oil derived polyurethane adhesives. European Polymer Journal 2018;101:291–303. doi:10.1016/j.eurpolymj.2018.02.041.
31. Zhou H, Liu H-Y, Zhou H, Zhang Y, Gao X, Mai Y-W. On adhesive properties of nano-silica/epoxy bonded single-lap joints. Materials & Design 2016;95:212–8. doi:10.1016/j.matdes.2016.01.055.
32. Malik M, Kaur R. Mechanical and Thermal Properties of Castor Oil-Based Polyurethane Adhesive: Effect of TiO2 Filler. Advances in Polymer Technology 2016;37:24–30. doi:10.1002/adv.21637.
33. Panchireddy S, Grignard B, Thomassin J-M, Jerome C, Detrembleur C. Bio-based poly(hydroxyurethane) glues for metal substrates. Polymer Chemistry 2018;9:2650–9. doi:10.1039/c8py00281a.
34. Oliveira PR, May M, Panzera TH, Scarpa F, Hiermaier S. Reinforced biobased adhesive for eco-friendly sandwich panels. International Journal of Adhesion and Adhesives 2020;98:102550. doi:10.1016/j.ijadhadh.2020.102550.
35. Minitab 18 Statistical Software. State College, PA: Minitab, Inc; 2017.
36. Design and Analysis of Experiments. John Wiley & Sons Inc; 2012.
37. ASTM E8 / E8M-16a - Standard Test Methods for Tension Testing of Metallic Materials. ASTM International, West Conshohocken, PA; 2016.
38. Mousa S, Kim G-Y. A direct adhesion of metal-polymer-metal sandwich composites by warm roll bonding. Journal of Materials Processing Technology 2017; 239:133–9. doi:10.1016/j.jmatprotec.2016.08.017.
39. Bruchhausen M, Holmström S, Simonovski I, Austin T, Lapetite J-M, Ripplinger S, et al. Recent developments in small punch testing: Tensile properties and DBTT. Theoretical and Applied Fracture Mechanics 2016;86:2–10. doi:10.1016/j.tafmec.2016.09.012.
40. Borsellino C, Bella GD, Ruisi V. Adhesive joining of aluminium AA6082: The effects of resin and surface treatment. International Journal of Adhesion and Adhesives 2009; 29:36–44. doi:10.1016/j.ijadhadh.2008.01.002.
41. ASTM C393 / C393M-16 - Standard Test Method for Core Shear Properties of Sandwich Constructions by Beam Flexure. ASTM International, West Conshohocken, PA; 2016.
42. ASTM D7250 / D7250M-16 - Standard Practice for Determining Sandwich Beam Flexural and Shear Stiffness. ASTM International, West Conshohocken, PA; 2016.
43. ASTM D790/15 - Standard Test Methods for Flexural Properties of Unreinforced and Reinforced Plastics and Electrical Insulating Materials. ASTM International, West Conshohocken, PA; 2015.

44. ASTM C20-15 - Standard Test Methods for Apparent Porosity, Water Absorption, Apparent Specific Gravity, and Bulk Density of Burned Refractory Brick and Shapes by Boiling Water ASTM International, West Conshohocken, PA; 2015.
45. Ashby MF. Materials selection in mechanical design. Amsterdam: Elsevier/Butterworth-Heinemann; 2017.
46. Akatay A, Bora MÖ, Fidan S, Çoban O. Damage characterization of three point bended honeycomb sandwich structures under different temperatures with cone beam computed tomography technique. Polymer Composites 2015;39:46–54. doi:10.1002/pc.23900.